

New All-Fused Ring Spiro Blue Host and Dopant System: Application in Sky-Blue Fluorescent Organic Light-Emitting Materials

Jae-Ryung Cha,[†] Chil-Won Lee,[‡] and Myoung-Seon Gong^{†,*}

[†]Department of Nanobiomedical Science and BK21 PLUS NBM Global Research Center, Dankook University, Chungnam 330-714, Republic of Korea. *E-mail: msgong@dankook.ac.kr

[‡]Department of Polymer Science and Engineering, Dankook University 126, Yongin 448-701, Republic of Korea

Received March 12, 2015, Accepted July 21, 2015, Published online October 4, 2015

Highly efficient sky-blue organic light emitting devices (OLEDs) were fabricated using fused-ring spiro host materials 1,10-di(2-naphthyl)spiro[benzo[*ij*]tetraphene-7,9'-fluorene] (**H1**) and 1-[1-(4-biphenyl)]-10-phenylspiro[benzo[*ij*]tetraphene-7,9'-fluorene] (**H2**). **H1** and **H2** were doped with a fluorescent dopant based on 5,9-di(di-*p*-tolylaminospiro[benzo[*c*]fluorene-7,9'-fluorene] (**D3**). Typical blue fluorescent OLEDs were fabricated with indium tin oxide (ITO)/N,N'-diphenyl-N,N'-bis[4-(phenyl-*m*-tolyl-amino)phenyl]-biphenyl-4,4'-diamine (DNTPD)/N,N,N',N'-tetra(1-biphenyl)-biphenyl-4,4'-diamine (TBB)/SBTF hosts: **D3**/9,10-di(naphthalene-2-yl)anthracene-2-yl-(4,1-phenylene)(1-phenyl-1*H*-benzo[*d*]imidazole) (LG201)/LiF/Al configuration and were subsequently investigated. The **H1**: 5%**D3** device exhibited an electroluminescent emission at 472 nm, with efficiency 6.91 cd/A, external quantum efficiency 4.56% at 107.84 mA/cm², and a sky-blue color at Commission Internationale de l'Éclairage (CIE) (*x*,*y*) coordinates of (0.150, 0.217) at 7447 cd/m².

Keywords: Fluorescence organic light emitting devices, Spirobenzo[*c*]fluorene-7,9'-fluorene, Spirobenzo[*ij*]tetraphene-7,9'-fluorene, Blue dopant, Blue host

Introduction

Over the last decade, highly efficient blue organic light emitting diodes (OLEDs) have attracted a considerable amount of attention due to their potential use in full-color flat-panel displays or in lighting sources.^{1–3} However, blue-emitting materials with high efficiency and pure, saturate color are difficult to design because of their wide bandgap. A number of anthracene, distyrylarylene, pyrene, fluorene, and silole derivatives have been presented in the literature as blue host materials,^{3–7} and among these, anthracene derivatives have played an important role in the development and application of host and dopant materials for OLED applications.^{8–11} However, the number of optimized blue dopant materials with energetic matching is still limited, except for monostyrylamine, distyrylamine, and iminodibenzyl-substituted distyrylarylenes.^{12–15}

Compounds with a spiro-sp³ carbon center are promising candidates for use in blue organic light-emitting materials because of their high energy gap and low highest occupied molecular orbital (HOMO) levels.¹² Spirobifluorene derivatives have received much attention because they not only prevent close packing and intermolecular interaction but also increase the molecular rigidity.^{16,17} As a result, spirobifluorene linkages have been introduced into the structure of the small molecules, leading to a reduction in the tendency to crystallize, improvement in the solubility, and an increase in the glass transition temperature.^{18–21}

In our previous study, we synthesized and characterized spiro[benzo[*c*]fluorene-7,9'-fluorene] (**SBFF**) derivatives with extended conjugated structures for use as blue host and dopant materials.^{22–26} These conjugated spiro molecules based on **SBFF** exhibited good thermal stability and unique optical and electrochemical properties that are desirable for use in new emitting materials for OLEDs technologies. In addition, the unique structure of highly conjugated spiro molecules allows their optical and electrochemical properties to be delicately tuned over a wide range through appropriate chemical modification to their aromatic moieties.^{27,28} Our study was extended to include a wider variety of fused ring spiro molecules, and spiro[benzo[*ij*]anthracene-7,9'-fluorene] (**SBAF**)^{28–31} and spiro[benzo[*ij*]tetraphene-7,9'-fluorene] (**SBTF**)^{32–36} units were introduced in blue OLEDs to improve their morphologic stability to achieve a highly efficient blue light emission.

Here, we report on the development of a sky-blue fluorescent dopant material 5,9-di(di-*p*-tolyl)aminospiro[benzo[*c*]fluorene-7,9'-fluorene] (**D3**), which was doped into morphologically stable fused ring host materials 1,10-dinaphthylspiro[benzo[*ij*]tetraphene-7,9'-fluorene] (**H1**) and 1-[1-(4-biphenyl)]-10-phenylspiro[benzo[*ij*]tetraphene-7,9'-fluorene] (**H2**). The **H1** and **H2** blue host materials employed an **SBTF** core structure to improve the light-emitting efficiency because of its extended conjugated structure, while the thermal and morphological stability were improved by implementing a twisted spiro structure. The

electroluminescence (EL) of devices using **H1** and **H2** host materials and **D3** dopant was investigated, and a high luminance efficiency of 6.91 cd/A and an external quantum efficiency (EQE) of 4.56% were demonstrated in the blue fluorescence of the sky-blue OLEDs.

Experimental

Materials and Measurements. Palladium(II) acetate, sodium *tert*-butoxide, tri-*t*-butylphosphine, and di-*p*-tolylamine (Aldrich Chemical Co., St. Louis, MO, USA) were used as received. Tetrahydrofuran and toluene were distilled over sodium and calcium hydride. 5,9-Dibromo-**SBFF** was prepared as previously reported.^{15,19} 1,10-Di(2-naphthyl)spiro[benzo[*ij*]tetraphene-7,9'-fluorene] (**H1**) and 1-[1-(4-biphenyl)]-10-phenylspiro[benzo[*ij*]tetraphene-7,9'-fluorene] (**H2**) were prepared by the methods reported previously.^{32–34} 9,10-Di(2-naphthyl)anthracene (β -ADN) was used as commercial host material. Photoluminescence (PL) spectra were recorded on a fluorescence spectrophotometer (Jasco FP-6500; Tokyo, Japan) and UV-vis spectra were obtained by a UV-vis spectrophotometer (Shimadzu, UV-1601PC, Tokyo, Japan). Energy levels were measured with a low-energy photoelectron spectrometer (AC-2; Riken-Keiki, Union City, CA, USA). FT-IR spectra were obtained with a Thermo Fisher Nicolet 850 spectrophotometer (Waltham, MA, USA), and elemental analysis were performed using a CE Instrument EA1110 (Hindley Green, Wigan, UK) apparatus. Differential scanning calorimetry (DSC) measurements were performed on a Shimadzu DSC-60 instrument under nitrogen. Thermogravimetric analysis (TGA) measurements were performed on a Shimadzu TGA-50 thermogravimetric analyzer. High-resolution mass spectra were recorded using an HP 6890 (Brea, CA, USA) and Agilent Technologies 5975C MSD in the fast atom bombardment (FAB) mode (Palo Alto, CA, USA).

Preparation of 5,9-di(di-*p*-tolyl)aminospiro[benzo[*c*]fluorene-7,9'-fluorene] (D3**).** 5,9-Dibromo-**SBFF** (1) (7.06 g, 13.47 mmol), di-*p*-tolylamine (5.31 g, 26.94 mmol) and palladium acetate (0.30 g, 1.35 mmol) were dissolved in anhydrous toluene (70 mL) under nitrogen atmosphere. To the reaction mixture was added a solution of tri-*t*-butylphosphine (0.55 g, 2.69 mmol) and sodium *t*-butoxide (3.24 g, 33.68 mmol) in toluene (70 mL) dropwise slowly. The reaction mixture was stirred for 3 days at 100 °C. Following the removal of the solvent *in vacuo*, an ammonia solution (70 mL) was added, and the mixture was left to stand for 2 h. Dichloromethane (150 mL) and water (100 mL) were added, and the organic phase was separated. The organic layer was dried over anhydrous MgSO₄ and evaporated *in vacuo* to give the crude product, which was purified by column chromatography by dichloromethane/hexane (v/v, 1/3). The final product was obtained as a yellowish green powder.

Yield 74%. ¹H NMR (500 MHz, CDCl₃) δ (ppm) 8.78–8.76 (d, J = 8.47 Hz, 1H, Ar-CH-naphthalene), 8.22–8.20 (d, J = 8.53 Hz, 1H, Ar-CH-naphthalene),

8.02–8.00 (d, J = 8.45 Hz, 1H, Ar-CH-benzene), 7.69–7.67 (d, J = 7.60 Hz, 2H, Ar-CH-fluorene), 7.60–7.58 (t, J = 8.00 Hz, 1H, Ar-CH-naphthalene), 7.39–7.37 (t, J = 7.57 Hz, 1H, Ar-CH-naphthalene), 7.28–7.26 (t, J = 7.90 Hz, 2H, Ar-CH-fluorene), 7.12–7.10 (s, 2H, Ar-CH-benzene), 7.12–7.10 (t, 4H, Ar-CH-benzene), 7.10–7.08 (d, 2H, Ar-CH-fluorene), 7.04–7.02 (d, 2H, Ar-CH-benzene), 6.96–6.94 (d, 1H, Ar-CH-benzene), 6.90–6.88 (t, 4H, Ar-CH-benzene), 6.88–6.86 (d, 2H, Ar-CH-naphthalene), 6.80–6.78 (d, 2H, Ar-CH-benzene), 6.74–6.72 (d, 2H, Ar-CH-benzene), 6.72–6.68 (d, 2H, Ar-CH-benzene), 2.08–2.09 (s, 12H, Ar-CH₃). ¹³C NMR (CDCl₃) δ 151.5, 148.1, 147.8, 147.5, 147.4, 146.8, 142.1, 139.0, 138.8, 136.9, 135.4, 131.9, 130.8, 129.2, 129.0, 128.8, 127.9, 126.9, 126.1, 125.7, 124.4, 124.1, 123.8, 123.6, 123.3, 123.0, 122.5, 122.1, 121.4, 121.1, 120.4, 119.2, 118.6, 77.4, 77.2, 76.9, 66.4, 21.4, 21.3. Anal. Calcd. for C₅₇H₄₄N₂ (M_w , 756.97): C, 90.44; H, 5.86; N, 3.70. Found: C, 90.38; H, 5.88; N, 3.67. MS (FAB) m/z 757.97 [($M + 1$)⁺]. UV-vis (THF): λ_{max} (Absorption) = 415 nm, λ_{max} (Emission) = 474 nm.

OLED Fabrication. A basic device configuration of indium tin oxide (ITO) (150 nm)/*N,N'*-di(1-naphthyl)-*N,N'*-bis[(4-diphenylamino) phenyl]-biphenyl-4,4'-diamine (DNTPB, 60 nm)/*N,N,N',N'*-tetra(1-biphenyl)-biphenyl-4,4'-diamine (TBB, 30 nm)/**SBTF** hosts: **D3** (30 nm, 5%) / 9,10-di(naphthalene-2-yl)anthracene-2-yl-(4,1-phenylene)(1-phenyl-1*H*-benzo[*d*]imidazole) (LG201, 20 nm)/LiF (1 nm)/Al (200 nm) was used for device fabrication. The organic layers were deposited sequentially onto the substrate at a rate of 1.0 Å/s by thermal evaporation from heated alumina crucibles. The concentration of the dopant materials was varied in steps of 5%. The devices were encapsulated with a glass lid and a CaO getter after cathode deposition. Current density–voltage luminance and EL characteristics of the blue fluorescent OLEDs were measured with a Keithley 2400 source measurement unit (Cleveland, OH, USA) and a CS 1000 spectroradiometer (Minota GmbH, Arensburg, Germany).

Results and Discussion

Synthesis and Characterization. Highly conjugated fused-ring spiro host materials **H1** and **H2** were prepared by multi-step synthetic routes, as previously reported (Figure 1).^{32–34} 5,9-Dibromo-**SBFF** was prepared by selective bromination of 5-bromo-**SBFF** in carbon tetrachloride solvent.^{15,19} The dopant material **D3** was prepared by amination reactions of 5,9-dibromo-**SBFF** with di(*p*-tolyl)amine in the presence of

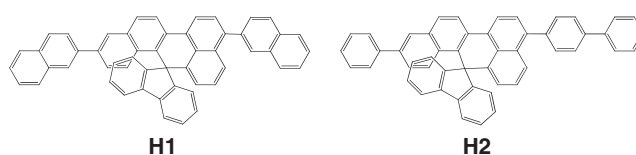
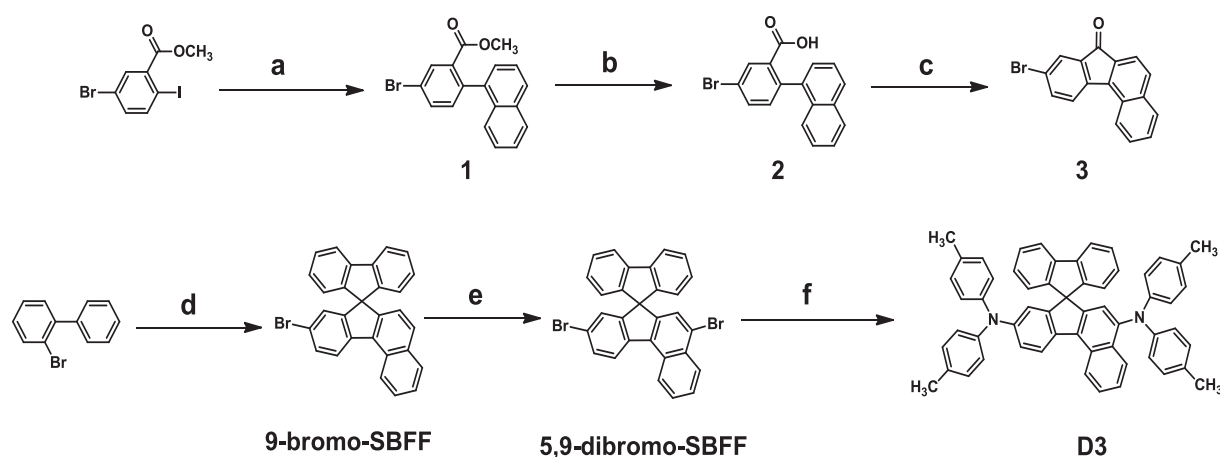


Figure 1. Chemical structure of **SBTF** host materials.



a: naphthalene-1-boronic acid/tetrakis(triphenylphosphine) palladium(0)/K₂CO₃/THF; b: NaOH/HCl/Ethanol; c: CH₃SO₃H/30°C/24 h; d: *n*-BuLi/-78°C/3/HCl/CH₃COOH; e: Br₂/CCl₄; f: di(*p*-tolyl)amine/palladium acetate

Figure 2. Preparation of SBFF dopant material.

a palladium catalyst as shown in Figure 2. The synthetic yield of **D3** was 74%. Chemical structures and compositions of the resulting SBFF dopant were characterized by ¹H-NMR, ¹³C-NMR, FT-IR spectroscopy, elemental analysis, and gas chromatography-mass spectrometry. The chiral carbon peak was observed at 60.0 ppm in the ¹³C-NMR spectra. Results of elemental analysis and mass spectrometry also supported formation of **D3** and matched well with the calculated data.

Optical Properties and Energy Levels. Figure 3(a) presents the UV-vis absorption and photoluminescence (PL) spectra of **D3** in a dilute solution (THF) and as a neat film on a quartz plate. The absorption bands at ~300 nm for **D3** originate from the diarylamine-centered *n*-π* transition. The absorption maximum of **D3** in dilute solution, centered at 415 nm, is similar to that provided by its thin film (421 nm), implying that no significant intermolecular interactions occur in the ground state. The PL maximum of **D3** was at 474 nm in solution, whereas in the solid-state PL maximum was observed at 479 nm. The nonplanar structure of **D3** facilitates its use as dopant in sky-blue OLEDs owing to the efficient inhibition of π-π* stacking in the film state.

The UV-vis absorption and PL spectra of the **H1** and **H2** host materials are summarized in Figure 3(b) and (c), and Table 1. **H1** and **H2** showed absorption peaks at 387 and 368 nm, respectively. PL maxima of **H1** and **H2** were at 440 and 441 nm in solution, respectively, whereas the solid-state PL maxima were observed at 445 nm for **H1** and 447 nm for **H2**. These solid-state PL spectra were slightly redshifted compared to those of other nonspiro molecules.³⁷

Thermal Properties. The molecular configuration of **D3** endowed it with high thermal stability, as indicated by a high decomposition temperature (*T*_d = 412 °C, corresponding to 5% weight loss during TGA) and a rather high glass transition temperature (*T*_g = 136 °C, determined using DSC). No

melting points were observed during the second heating, even though the sample was given enough time to cool in air. Once the sample had become an amorphous solid, it did not revert to a crystalline state. As a result, **D3** forms homogeneous and stable amorphous films upon thermal evaporation. The *T*_d values of **H1** and **H2** were 428 and 439 °C, respectively, whereas their *T*_g values were 179 and 168 °C, respectively. *T*_g of **H1** was increased by 11 °C compared to that of **H2** because of the 2-naphthyl moiety at both 5- and 9-position.

Theoretical Calculations and Energy Levels. To gain more insight into the electronic structure of **D3**, density function theory (DFT) calculations were performed at Beck's three-parameter Lee-Yang-Parr (B3LYP) functional with 6-31G* level for the geometry optimization. As shown in Figure 4, the HOMO of **D3** is mainly populated over both the di(*p*-tolyl)amine and SBAF with considerable contribution, whereas the lowest unoccupied molecular orbital (LUMO) has a sizable contribution from the SBAF core. The di(*p*-tolyl)amine at the 5-position of **D3** was twisted with respect to the naphthalene plane, with a dihedral angle of 52°, whereas the di(*p*-tolyl)amine at the 9-position of **D3** was twisted with respect to the phenylene plane with a dihedral angle of 38°. Using low-energy photoelectron spectroscopy, we estimated the energy level of HOMO to be 5.29 eV. The crossing point of the background and the yield line is the photoemission threshold energy, also called the work function or the ionization potential, as shown in Figure 5.³⁸ By subtracting the optical energy gap (*E*_g = 3.12 eV) from the HOMO energy level, we calculated the energy level of LUMO to be 2.53 eV. The HOMO of **H1** and **H2** was also calculated from the photoemission threshold energy curve. The HOMO and LUMO energy levels were 5.82 and 2.82 eV for **H1** and 5.75 and 2.73 eV for **H2**, respectively. Figure 6 shows the energy levels

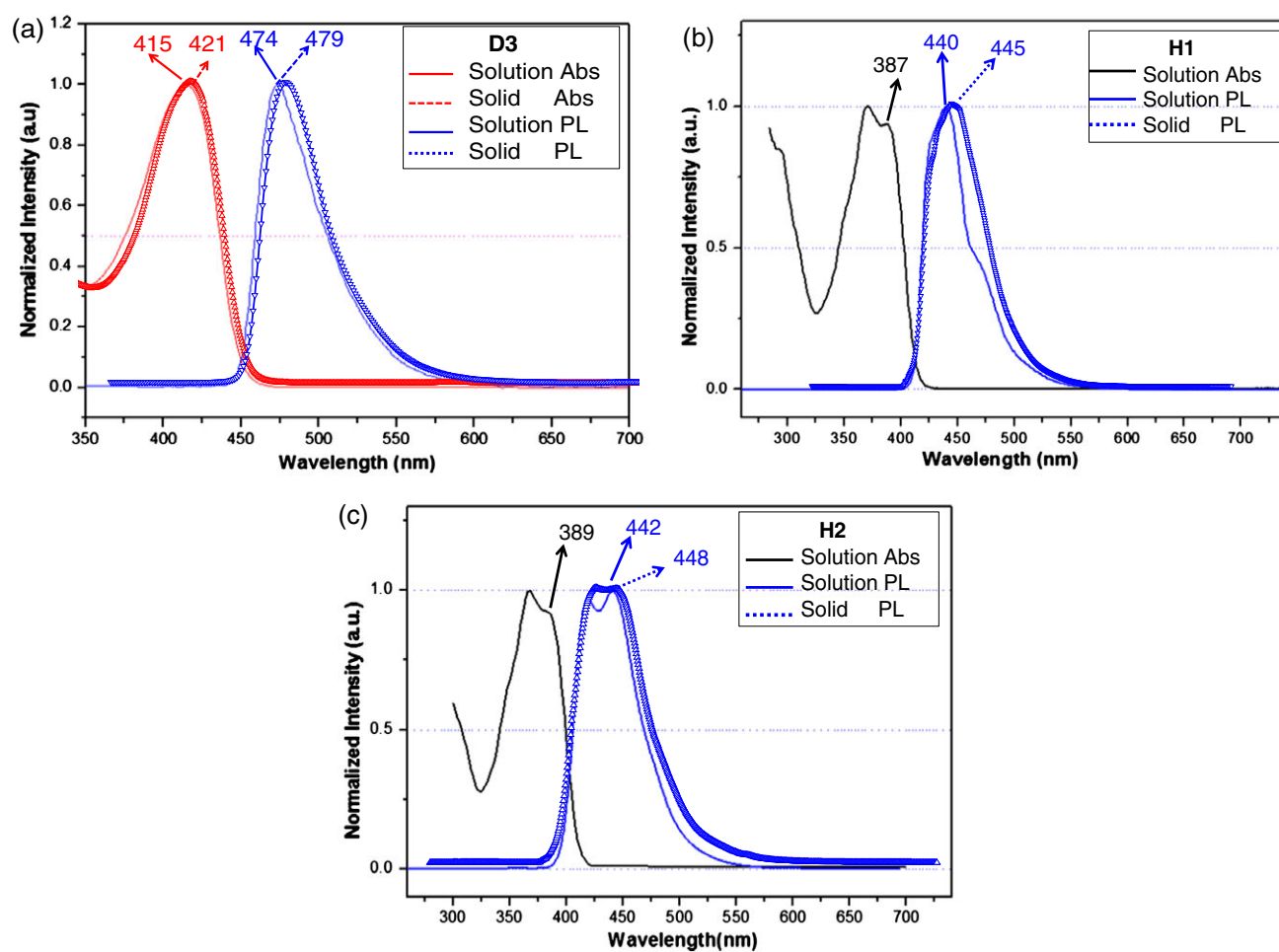


Figure 3. UV-vis and PL spectra of (a) D3, (b) H1, and (c) H2.

Table 1. UV absorption, PL, energy levels, and thermal properties of two SBTF hosts and SBFF dopant.

Sample properties			H1	H2	D3
Purity ^a	HPLC	(%)	99.9	99.9	99.26
Thermal analysis	DSC	T_g^b (°C)	179	168	136
		T_d^c (°C)	428	439	412
Optical analysis	UV (THF)	Maximum (nm)	387	389	415
	PL (THF)	Maximum (nm)	440	441	474
		FWHM ^d (nm)	43	63	47
	PL (Solid)	Maximum (nm)	445	447	479
		FWHM ^d (nm)	54	67	58
		B_g^e (eV)	3.00	3.02	2.70
Electrical analysis	AC-2 ^f	HOMO (eV)	5.82	5.75	5.29
		LUMO (eV)	2.82	2.73	2.53

^a The purity of the samples were finally determined by high-performance liquid chromatography (HPLC) using the prepared samples above after train sublimation.

^b Glass transition temperature.

^c Decomposition temperature.

^d Full width at half-maximum.

^e Bandgap.

^f photoelectron spectroscopy (60 nm film).

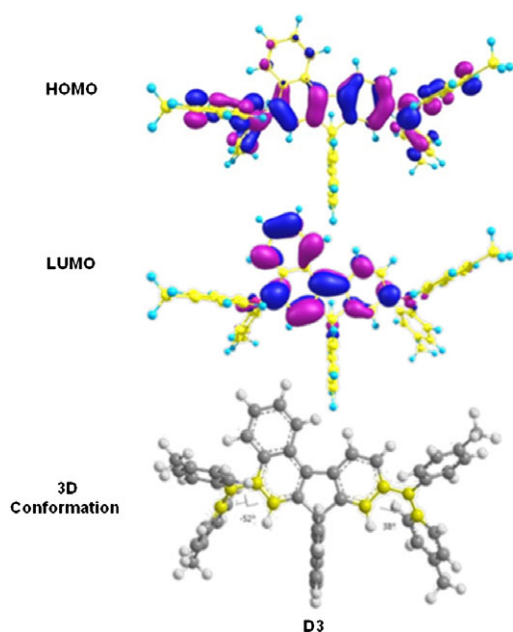


Figure 4. HOMO and LUMO electronic density distributions of SBFF dopant material **D3**, calculated at the DFT/B3LYP/6-31G* level for optimization and time-dependent DFT (TDDFT) using Gaussian 03 (Gaussian, Inc., Wallingford, CT, USA).

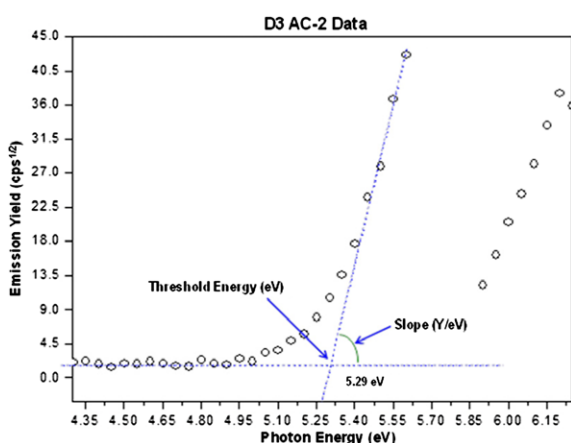


Figure 5. Low-energy photoelectron spectra (from AC-2) of the SBFF dopant **D3**.

of devices using the **H1** and **H2** hosts and **D3** as dopant materials.

EL Properties. Figure 7 shows the normalized EL spectra of a device composed of **H1**, **H2**, and β -ADN doped with 5% **D3** at 7 V. All the devices showed an intense sky-blue emission in the EL spectra at 472 nm for **H1**, 468 nm for **H2**, and 468 nm for β -ADN. The devices **H1** showed a 4 nm longer wavelength in the EL spectra than **H2**.

Looking at the EL spectra for all three hosts, we can conclude that there is almost exclusively emission from the dopant with a neat single peak ($\lambda_{\text{max}} = 474$ nm) in THF, suggesting that the energy transfer from the host to **D3** dopant was quite efficient at the optimum dopant concentration employed in this experiment. Sky-blue emission was observed, and the

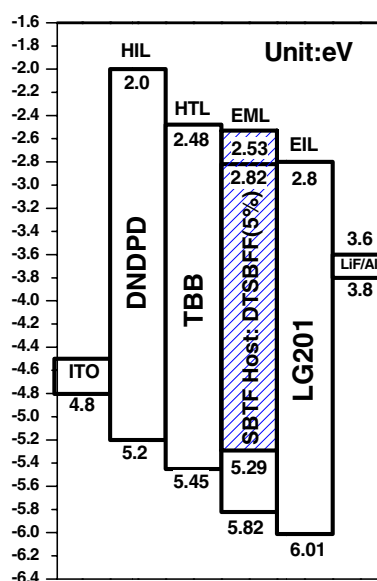


Figure 6. Energy diagram of the blue fluorescence device using SBTF host doped with SBFF dopant.

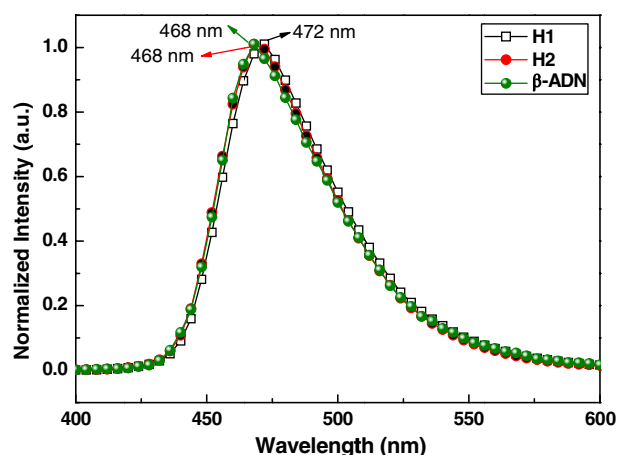


Figure 7. Electroluminescence spectra of **H1**, **H2**, and β -ADN devices doped with **D3**.

Commission Internationale de l'Éclairage (CIE) color coordinates of the devices based on **H1**, **H2**, and β -ADN were (0.150, 217), (0.136, 0.202), and (0.139, 0.208), respectively. This apparent resistance to color change under various drive current densities suggests that the charge carriers for recombination are well balanced in this blue emitter and both excitation mechanism of charge trapping and Förster energy transfer may be prevalent in the **D3** doped devices.

OLED Device Properties. The device structure used was ITO (150 nm)/DNDPD (HIL, 60 nm)/TBB (HTL, 30 nm)/SBTF hosts: **D3** (30 nm, 5%)/LG201 (ETL, 20 nm)/LiF (1 nm)/Al (200 nm), where the emitting layer was composed of the fluorescent dopant **D3** and hosts **H1**, **H2**, and β -ADN. The current density–voltage–luminance characteristics of the devices with three hosts doped with 5% **D3** dopant are shown in Figure 8. All devices show the typical characteristics of OLEDs, and the turn-on voltages of devices **H1**, **H2**,

and β -ADN were 3.6, 3.6, and 4.0 V, respectively. It is found that the luminance is higher for the device **H1** than for the device **H2** at the same driving voltage. The maximum brightness of the devices **H1** and **H2** was 7447 and 5798 cd/m^2 , which is an improvement over the device β -ADN with 812 cd/m^2 due to the different hole–electron recombination probability in the emitting layer for each blue OLED. In addition, β -ADN showed much lower current density characteristics than the two **SBTF** hosts **H1** and **H2**.

Devices **H1** and **H2** have the small energy gap of 3.00 and 3.02 eV (β -ADN = 3.03 eV) between HTL and ETL, which makes it easier for electron injection from the ETL to the emitting layer, thereby able to reach the high luminance efficiency (Figure 9). We believe that the more balanced carriers for recombination in the **H1** and **H2** devices may be another reason for the enhanced luminance efficiency in addition to the more effective Förster energy transfer.³⁹

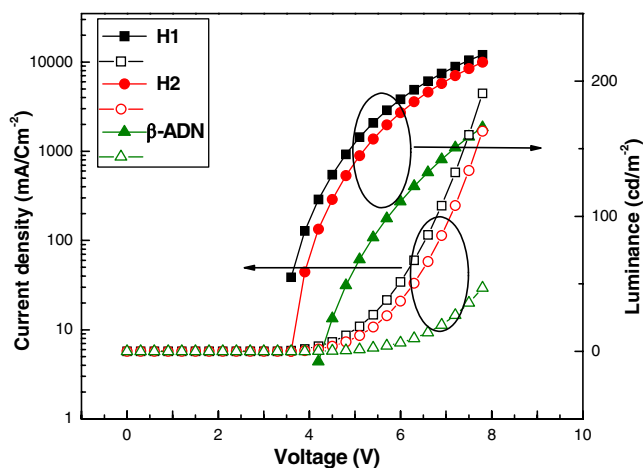


Figure 8. Current density–voltage–luminescence characteristics of the devices using **H1**, **H2**, and β -ADN host materials doped with 5% **D3**.

Figure 10(a) presents the quantum efficiency–luminance and power efficiency–luminance curves of the sky-blue OLEDs. The quantum efficiency was also dependent on the host materials, and the device using β -ADN doped with **D3** showed a lower efficiency than the devices **H1** and **H2**. It is noteworthy that we obtained an almost upper EQE of 5.20% at 5.1 V in the device **H2** based on the fluorescent dopant **D3**. The device **H2** shows higher EQE than the device **H1** (5.10%) although the device **H2** shows lower luminance efficiency than the device **H1** at a fixed voltage.

The power efficiency of the sky-blue OLEDs is also shown in Figure 10(b). In spite of the low quantum efficiency of the device **H1**, the power efficiency of the device **H1** was higher than that of the device **H2**. The power efficiency at a low current density of 48.57 cd/m^2 was 6.6 lm/W , which is much higher than that of β -ADN (3.0 lm/W) (Table 2).

The dependence of the chromaticity of the device on the current density was measured to evaluate its stability (Figure 11).

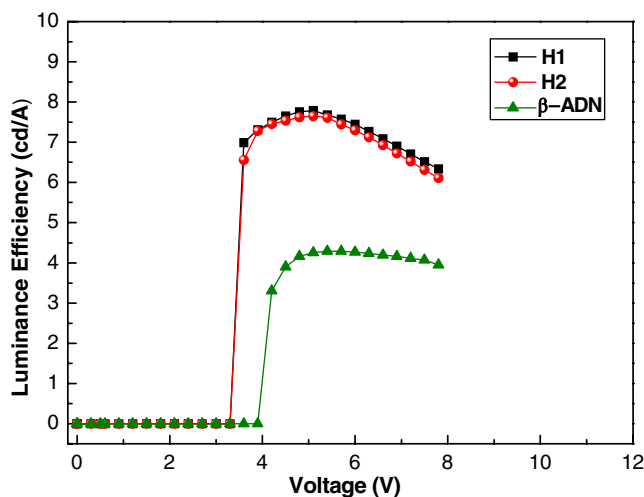


Figure 9. Luminance efficiency–voltage characteristics of the device using **H1**, **H2**, and β -ADN host materials doped with 5% **D3**.

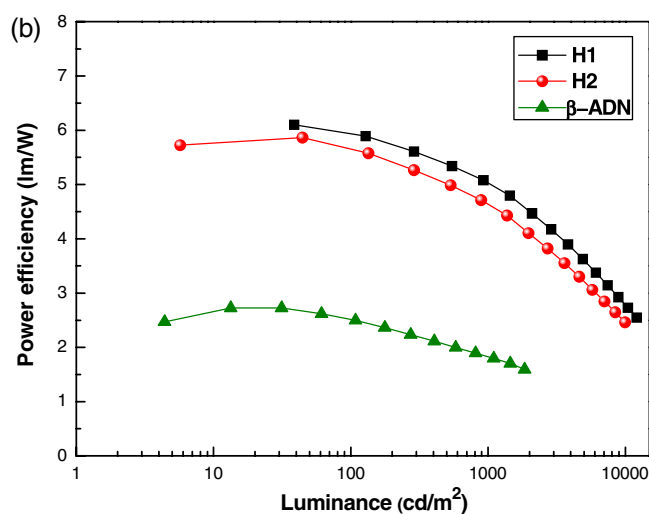
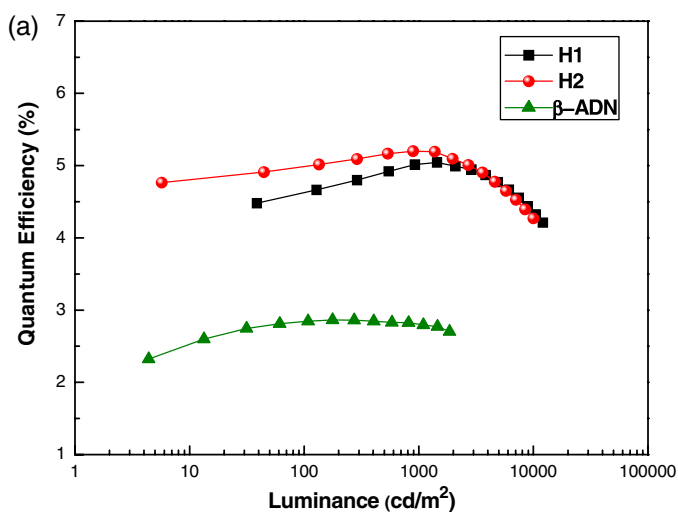
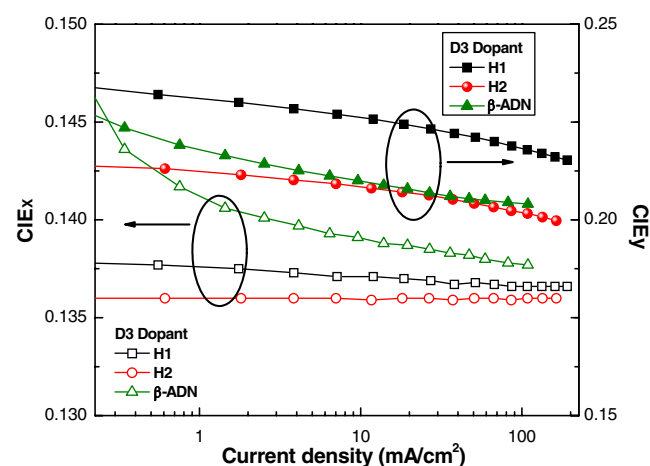


Figure 10. (a) Quantum efficiency–luminance and (b) power efficiency–luminance curves of the sky-blue light-emitting diodes.

Table 2. Electroluminescence properties of the devices obtained from **SBTF** hosts and **SBFF** dopant materials.

Material properties	Host dopant ^a	H1	H2	β -ADN
		D3		
EL at 7 V	λ_{\max} (nm)	472	468	468
	FWHM (nm)	50	50	51
	J (mA/cm ²)	107.84	85.70	19.50
	L^b (cd/m ²)	7447	5758	812
	LE ^c (cd/A)	6.91	6.72	4.16
	LE (cd/A) ^d	7.78 (5.1 V)	7.65 (5.1 V)	4.29 (5.4 V)
	EQE ^b (%)	4.56	4.65	2.82
	EQE ^e (%) ^d	5.04 (5.1 V)	5.20 (5.1 V)	2.86 (5.7 V)
	PE ^f (%)	3.14	3.06	1.90
	PE ^f (%) ^d	6.10(3.6 V)	5.72 (3.6 V)	2.72 (4.8 V)
	CIE-x	0.150	0.136	0.139
	CIE-y	0.217	0.202	0.208

^a 5% concentration.^b Luminance.^c Luminance efficiency.^d Values at a highest peak.^e External quantum efficiency.^f Power efficiency.**Figure 11.** Stability of the chromaticity depicted by CIE coordination for the devices using **H1** and **H2** hosts doped with 5% **D3** dopant.

The CIE chromatic variation of **H1** and **H2** devices is negligible ($x = 0.001$, $y = 0.01$) with the current density increasing from 5 to 100 mA/cm². When β -ADN and 5% **D3** dopant were used, the color stability was even worse: its chromatic variation was ($x = 0.002$, $y = 0.012$). According to the color stability of **SBTF**-based devices, we can confirm that the energy levels of **SBTF** hosts and **SBFF** dopant match well with neighboring layers, and the charge carrier recombination at the emitting layer is efficient at all current densities.³⁸ Device **H2** shows a near-flat color variation versus current density and is resistant to color shift with increasing current density as well. Based on these results, we attribute this apparent resistance to color shift to the inserted spiro linking group, which effectively prevents the dyes from aggregation at high concentration.³⁸

The sky-blue dopant **D3** had a large capacity to catch the holes, and thus minimize the loss of holes resulting in good

EL efficiency. Thus, the HOMO level of **D3** was suitable for hole-trapping and hole transportation as a dopant, and the **SBTF** hosts were moderate for balancing holes and electrons in the emitting layer. It is therefore evident that the overlap between the hypsochromic-shifted emission peak of **H1** and **H2** and the absorption peak of **D3** is better than that of commercial β -ADN, which is essential for efficient Förster energy transfer.

Conclusion

In conclusion, we designed and prepared a new **SBFF** derivative **D3**, which is a thermally stable and highly fluorescent blue dopant material because of its rigid and spiro molecular structure. The fused ring host materials **H1** and **H2** doped with **D3** devices show blue emissions with the maximum peak at 472 nm and have the EL spectra identical to the PL spectrum of **D3**. The ITO (150 nm)/DNTPB (60 nm)/TBB (30 nm)/**H1** hosts: **D3** (30 nm, 5%)/LG201 (20 nm)/LiF (1 nm)/Al (200 nm) device displayed sky-blue emission, a maximum EQE of 4.56%, a maximum luminance efficiency of 6.91 cd/A at the current density of 107.84 mA/cm², and maximum luminance of 7447 cd/m².

References

1. S. R. Forrest, *Org. Electron.* **2003**, *4*, 45.
2. C. H. Liao, M. T. Lee, C. H. Tsai, C. H. Chen, *Appl. Phys. Lett.* **2005**, *86*, 203507.
3. J. M. Shi, C. W. Tang, *Appl. Phys. Lett.* **2002**, *80*, 3201.
4. Y. H. Kim, D. C. Shin, S. H. Kim, C. H. Ko, H. S. Hu, Y. D. Chae, S. K. Kwon, *Adv. Mater.* **2001**, *13*, 1690.
5. C. Hosokawa, H. Higashi, H. Nakamura, T. Kusumoto, *Appl. Phys. Lett.* **1995**, *67*, 3853.

6. C. C. Yeh, M. T. Lee, H. H. Chen, C. H. Chen, *J. Soc. Inf. Disp.* **2004**, *35*, 789.
7. A. Saitoh, N. Yamada, M. Yashima, K. Okinaka, A. Seno, K. Ueno, D. Tanaka, R. Yashiro, *J. Soc. Inf. Disp.* **2004**, *35*, 150.
8. W. J. Shen, R. Dodda, C. C. Wu, F. I. Wu, T. H. Liu, H. H. Chen, C. H. Chen, C. F. Shu, *Chem. Mater.* **2004**, *16*, 930.
9. J. Huang, J. H. Su, H. J. Tian, *Mater. Chem.* **2012**, *22*, 10977.
10. M. T. Lee, H. H. Chen, C. H. Lian, C. H. Tsai, C. H. Chen, *Appl. Phys. Lett.* **2007**, *85*, 3301.
11. Z. Q. Gao, B. X. Mi, C. H. Chen, K. W. Cheah, Y. K. Cheng, W. S. Wen, *Appl. Phys. Lett.* **2007**, *90*, 123506.
12. C. C. Wu, Y. T. Lin, K. T. Wong, R. T. Chen, Y. Y. Chien, *Adv. Mater.* **2004**, *16*, 61.
13. M. H. Ho, C. M. Chang, T. Y. Chu, T. M. Chen, C. H. Chen, *Org. Electron.* **2008**, *9*, 101.
14. M. T. Lee, C. H. Liao, C. H. Tsai, C. H. Chen, *Adv. Mater.* **2005**, *17*, 2493.
15. Y. M. Jeon, J. Y. Lee, J. W. Kim, C. W. Lee, M. S. Gong, *Org. Electron.* **2010**, *11*, 1844.
16. J. Salbeck, N. Yu, J. Bauer, F. Weissörtel, H. Bestgen, *Synth. Met.* **1997**, *91*, 209.
17. N. Johansson, J. Salbeck, J. Bauer, F. Weissörtel, P. Bröms, A. Andersson, W. R. Salaneck, *Adv. Mater.* **1998**, *10*, 1136.
18. C. W. Ko, Y. T. Tao, *Synth. Met.* **2002**, *126*, 37.
19. M. S. Gong, H. S. Lee, Y. M. Jeon, *J. Mater. Chem.* **2010**, *20*, 10735.
20. Y. M. Jeon, J. W. Kim, C. W. Lee, M. S. Gong, *Dye Pigment.* **2009**, *83*, 66.
21. F. C. Chen, Y. Yang, M. E. Thompson, J. Kido, *Appl. Phys. Lett.* **2002**, *80*, 2308.
22. S. O. Jeon, K. S. Yook, C. W. Joo, J. Y. Lee, *Org. Electron.* **2010**, *11*, 881.
23. J. A. Seo, C. W. Lee, M. S. Gong, *Dye Pigment* **2013**, *96*, 211.
24. C. W. Lee, J. G. Jang, M. S. Gong, *Dyes Pigments* **2013**, *98*, 471.
25. S. E. Jang, S. O. Jeon, Y. J. Cho, K. S. Yook, J. Y. Lee, *J. Luminescence* **2010**, *30*, 2184.
26. J. A. Seo, C. W. Lee, M. S. Gong, *Bull. Korean Chem. Soc.* **2013**, *34*, 1414.
27. Y. Wang, Q. Peng, Q. Hou, K. Zhao, Y. Liang, B. Li, *Theor. Chem. Acc.* **2011**, *129*, 257.
28. H. Liang, X. Wang, X. Zhang, Z. Ge, X. Ouyang, S. Wang, *Dyes Pigments* **2014**, *108*, 57.
29. J. Y. Kim, C. W. Lee, J. G. Jang, M. S. Gong, *Dyes Pigments* **2012**, *94*, 304.
30. M. J. Kim, C. W. Lee, M. S. Gong, *Dyes Pigments* **2014**, *105*, 202.
31. H. Liang, X. Wang, X. Zhang, Z. Liu, Z. Ge, X. Ouyang, S. Wang, *New J. Chem.* **2014**, *38*, 4696.
32. M. J. Kim, C. W. Lee, M. S. Gong, *Org. Electron.* **2014**, *15*, 2922.
33. M. J. Kim, C. W. Lee, M. S. Gong, *Bull. Korean Chem. Soc.* **2014**, *35*, 1639.
34. J. R. Cha, C. W. Lee, M. S. Gong, *J. Fluoresc.* **2014**, *24*, 1215.
35. J. R. Cha, C. W. Lee, M. S. Gong, *New J. Chem.* **2015**, *39*, 3813.
36. J. R. Cha, C. W. Lee, M. S. Gong, *Dyes Pigments* **2015**, *120*, 251.
37. X. Li, D. -Y. Wei, S. -J. Huang, Y. -Q. Zheng, *J. Solid State Chem.* **2009**, *182*, 95.
38. C. J. Cramer, D. G. Truhlar, *Phys. Chem. Chem. Phys.* **2009**, *11*, 10757.
39. I. Cho, S. H. Kim, J. H. Kim, S. Park, S. Y. Park, *J. Mater. Chem.* **2012**, *22*, 123.